



# Transverse Oscillation of Coronal Loops Induced by Eruptions of a Magnetic Flux Tube and a Plasmoid

K. Safna Banu<sup>1</sup> · Ram Ajor Maurya<sup>1</sup> · P.T. Jain Jacob<sup>1</sup>

Received: 7 May 2022 / Accepted: 6 September 2022 / Published online: 14 October 2022  
© The Author(s), under exclusive licence to Springer Nature B.V. 2022

## Abstract

We studied transverse oscillations in hot coronal loops of active region NOAA 12673 located at the west limb. Loop oscillations were associated with a plasmoid ejection from the same location. During the rising phase of the plasmoid, a magnetic flux tube was seen to be rising and bending towards the loop system that erupted before the plasmoid ejection. In addition to the plasmoid ejection, a large coronal mass ejection (CME) and an X8.2 flare were observed in the same active region for several hours ( $\approx 7$  hours). After the plasmoid ejection, a follow-up shock wave from the flare site was triggered by a sudden momentum transfer towards the solar disk. It was found to be propagating across the entire solar disk with an average speed of  $\approx 1290 \text{ km s}^{-1}$ . By analyzing the time sequence of these events, we found that a plasmoid ejection perturbed the loops from their equilibrium and set them in oscillation. We found different oscillations of the fundamental mode in two loops, fast decaying (with a period of 7.93 minutes and an average damping time of  $\approx 19$  minutes) and slow decaying (with a period of 6.31 minutes and an average damping time of  $\approx 34$  minutes). The two different oscillations could be due to their lengths, magnetic fields, and plasma densities. Using the methods of coronal seismology, we estimated the average magnetic field in the coronal loops to be 29 G and 36 G, which is consistent with the order of the coronal magnetic fields found in other studies.

**Keywords** Corona, structures · Flares, preflare phenomena · Flares, waves · Waves, magnetohydrodynamic · Waves, shock

## 1. Introduction

Coronal loops are closed magnetic structures in the form of arches embedded in the coronal plasma. They are rooted in the interior below the photosphere and are affected by the dynamics of the interior plasma and the activity in the atmosphere. However, it is still a mystery as

---

✉ R.A. Maurya  
[ramajor@nitc.ac.in](mailto:ramajor@nitc.ac.in)

K. Safna Banu  
[safna\\_p180029ph@nitc.ac.in](mailto:safna_p180029ph@nitc.ac.in)

P.T. Jain Jacob  
[jain\\_p180130ph@nitc.ac.in](mailto:jain_p180130ph@nitc.ac.in)

<sup>1</sup> Department of Physics, National Institute of Technology Calicut, Kerala 673601, India

to what drives them to be vertically standing against the strong solar gravity. They are found to be swaying during energetic activity such as flares, coronal mass ejections (CMEs), etc.

Solar flares are the result of the magnetic reconnection—tangling, crossing, and reorganization of magnetic field lines (Shibata, 1996) in which the magnetic energy is transformed into kinetic energy of rapidly moving CMEs, particle acceleration, and thermal energy to heat the plasma (Yokoyama et al., 2001). A preflare event can also trigger a large flare on a stable flux tube that destabilizes flux ropes (Nindos et al., 2015; Mitra and Joshi, 2019) and can initiate waves and oscillations in coronal loops. Standing kink-mode oscillations can be produced by the reconnection processes that lead to the formation of postflare loops and subsequently release (or even push down) of loops from the top (White, Verwichte, and Foullon, 2012), interactions of contracting loops with underlying loops (Russell, Simões, and Fletcher, 2015), ejection of jets or plasmoids from the flaring site (Zimovets and Nakariakov, 2015), and an eruption of a filament or flux rope. Coronal-loop oscillations may also be generated by shock waves (Aschwanden et al., 1999; Nakariakov et al., 1999; Hudson and Warmuth, 2004; Jain, Maurya, and Hindman, 2015). However, numerical simulations have shown that it is difficult to excite perturbations of the observed displacement amplitude of several minor radii of the loop (McLaughlin and Ofman, 2008; Ofman, 2009). Therefore, it is interesting to investigate the mechanism responsible for triggering the oscillations.

Flare-induced transverse coronal-loop oscillations were initially reported by Aschwanden et al. (1999) using observations provided by the *Transition Region and Coronal Explorer* (TRACE), and later using the observations provided by the *Atmospheric Imaging Assembly* (AIA) on board the *Solar Dynamic Observatory* (SDO) (Aschwanden and Schrijver, 2011), and by some other researchers (Nakariakov et al., 2021). They found the period of oscillations to be around 6.3 minutes with a quality factor  $\gg 4$ , in vertically polarized mode. The oscillation period is proportional to the length of the loops with exponential damping (Goddard et al., 2016). These oscillations attenuate gradually after a few periods due to different damping processes, such as cooling of the plasma (Aschwanden and Terradas, 2008). The resonant absorption is the leading mechanism to explain the damping of the transverse oscillations of loops (Hollweg and Yang, 1988; Goossens, Andries, and Aschwanden, 2002; Ruderman and Roberts, 2002).

Most of the reported coronal-loop oscillations are fast asymmetric kink oscillations (Nakariakov and Verwichte, 2005). The kink-mode oscillations are classified into two types: high amplitude with a decaying oscillation and low amplitude with decayless oscillation (Wang et al., 2012; Anfinogentov, Nisticò, and Nakariakov, 2013; Nisticò, Nakariakov, and Verwichte, 2013). These oscillations are generally periodic displacements of coronal loops and are in the fundamental mode (Nakariakov et al., 1999; Jain, Maurya, and Hindman, 2015). In some events, the harmonics have also been reported (Moortel and Brady, 2007; Doorsselaere, Nakariakov, and Verwichte, 2007; White and Verwichte, 2012). These oscillations can be used to study the physical properties of the coronal plasma.

The information on the coronal magnetic field is essential as it provides an understanding of solar activity in its atmosphere. The direct measurement of coronal magnetic fields using standard techniques such as the Zeeman effect is inadequate due to the weak field strength. However, other techniques such as the polarization of the microwave waves (Brosius et al., 1997; Ryabov et al., 1999) and radio waves (Gelfreikh, 1999; Ryabov et al., 2005) have successfully been used to measure the coronal magnetic fields, called coronal magnetography. Coronal waves and oscillations provide us an indirect method to diagnose the plasma properties similar to the helioseismology for the solar interior. They can be used to estimate the physical parameters of the solar corona, such as internal Alfvén speed, magnetic-field strength and density structures of coronal loops. For more details about the recent reports on

the observations and theoretical modeling of coronal oscillations, the reader may refer to a recent review article by Nakariakov et al. (2021).

This paper analyzes the properties of transverse oscillations of two coronal loops observed by SDO/AIA. Close to the oscillating loops, we found flux tubes rising, the ejection of a plasmoid, flares, shock waves, and a CME. One of these events triggered the oscillation in coronal loops. Initially, we investigated the source of their excitation by analyzing the intensity variations associated with these events. Further, using oscillation properties, we estimated the kink speed and the magnetic field in the coronal loops. Section 2 provides a detailed description of the observational data used. The analysis and results are presented in Section 3. Finally, the summary and discussions are given in Section 4.

## 2. Observational Data

For this study, we used the observations provided by the SDO/AIA, specifically, the extreme ultraviolet (EUV) 171-Å intensity images of 10 September 2017 from 15:00 UT to 17:00 UT. The EUV 171-Å intensity images show emissions mainly in Fe IX from the solar plasma at the upper transition region and quiet corona at temperature  $T \approx 0.63$  MK (O'Dwyer et al., 2010; Lemen et al., 2011). These observations are taken with a pixel resolution of  $0''.6$  and a temporal resolution of 12 s. To study the flare energetics in X-rays, we also utilized the *Geosynchronous Operational Environmental Satellites* (GOES) observations in the 0.5–4.0 Å and 1.0–8.0 Å wavelength bands. The flare-associated CME was analyzed using the data obtained from the C2 and C3 coronagraphs of the *Large Angle and Spectrometric Coronagraph* (LASCO) (Brueckner et al., 1995) on board the *Solar and Heliospheric Observatory* (SOHO).

Using the SDO/AIA observations, some researchers studied the activity associated with this event. For example, Seaton and Darnel (2018) reported a flux-rope emergence, the structure of a coronal cavity, and associated current-sheet formation. The EUV waves associated with this event that covered the entire solar disk were reported earlier by Liu et al. (2018). Using the SOHO/LASCO CME observations, Gopalswamy et al. (2018) found a fast-propagating halo CME associated with the main flare. We analyzed the transverse coronal loop oscillation, the cause of this oscillatory event and estimated the physical parameters.

## 3. Analysis and Results

The results of our analysis are shown in Figures 1–11.

### 3.1. The Active Region and the Oscillating Coronal Loops

The active region NOAA 12673 emerged in the far side of the solar disk, and it was first observed as a simple sunspot region at the east limb at around S8 (8° south) on 28 August 2017. It evolved into a complex active region during 9–10 September 2017 while crossing the disk near the west limb (see Figure 1). It produced several energetic flares, such as 38 C-class, 20 M-class, and 2 X-class, during its disk transit from the east to the west limb. The line-of-sight magnetic field in the active region at and before the day of the initiation of an X8.2 flare (10 September 2017) is shown in Figure 1 (bottom panel). On 10 September, most of the active region (panel d) is located on the far side of the solar disk, which prevented us from analyzing the activity-related changes at the photosphere. However, the coronal loops

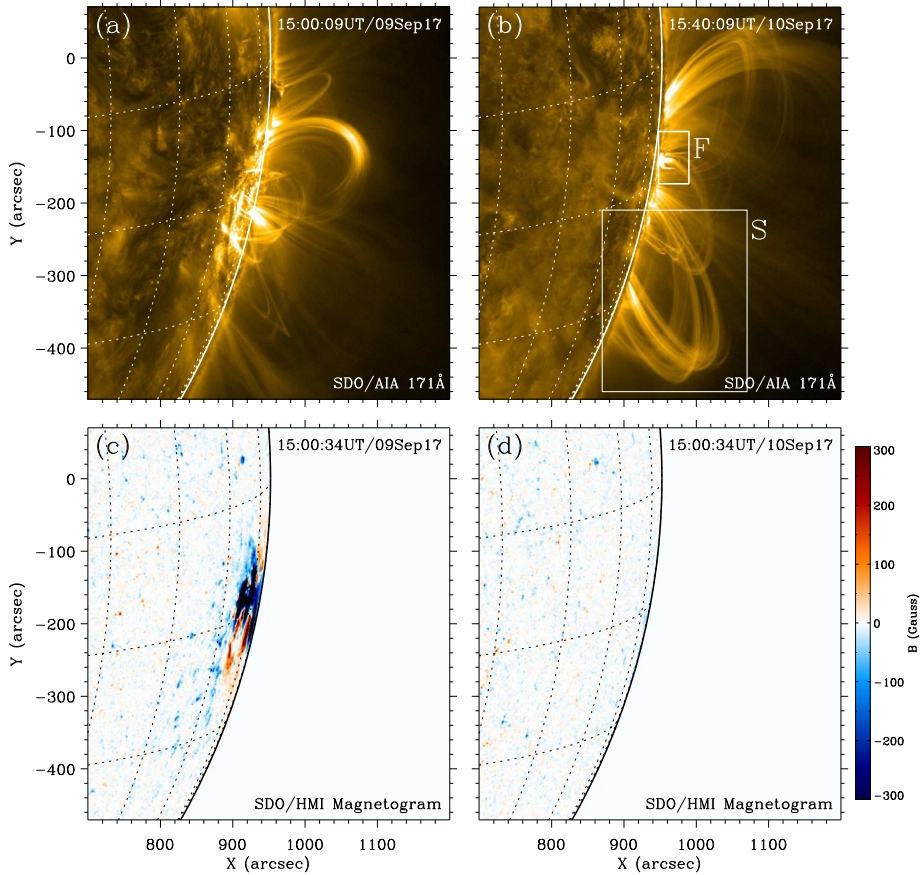


**Figure 1** A sample of the SDO/AIA 171-Å intensity images (top row) and the SDO/HMI magnetograms (bottom row) covering the active region NOAA 12673 and associated coronal loops. In panel c, the small box ‘F’ marks the flare site, and the box ‘S’ represents the coronal loops that are considered to study the oscillations.

associated with the active region can be seen in AIA EUV observations, such as the 171-Å intensity images (panel b), because of their heights above the photosphere.

The oscillating coronal loops (marked by the box ‘S’) are located southward from the flare site (labeled by ‘F’). These coronal loops were almost visible in all AIA passbands such as 171 Å, 211 Å, 193 Å, and 131 Å, weakly in 335 Å and 94 Å (see Figure 2), which indicates that the loops had a temperature distribution of 0.3 to 2 MK and most of them were warm loops. They seem to be inclined towards the south from the vertical. A careful analysis of the magnetograms taken a few days before the flare and EUV images showed that the footpoints of these loops were rooted in the same active region. This region had mixed magnetic polarities. A dominant negative (positive) polarity region was found to be located to the north (south) of the active region center. There were diffused magnetic fields with opposite polarities in the nearby regions. There were no other active regions in its neighborhood. The coronal loops marked by the box ‘S’ were part of this active region. One of the footpoints of these loops was located near the center of the active region and the other in the diffused magnetic-polarity regions to the south. The X8.2 flare is seen in the

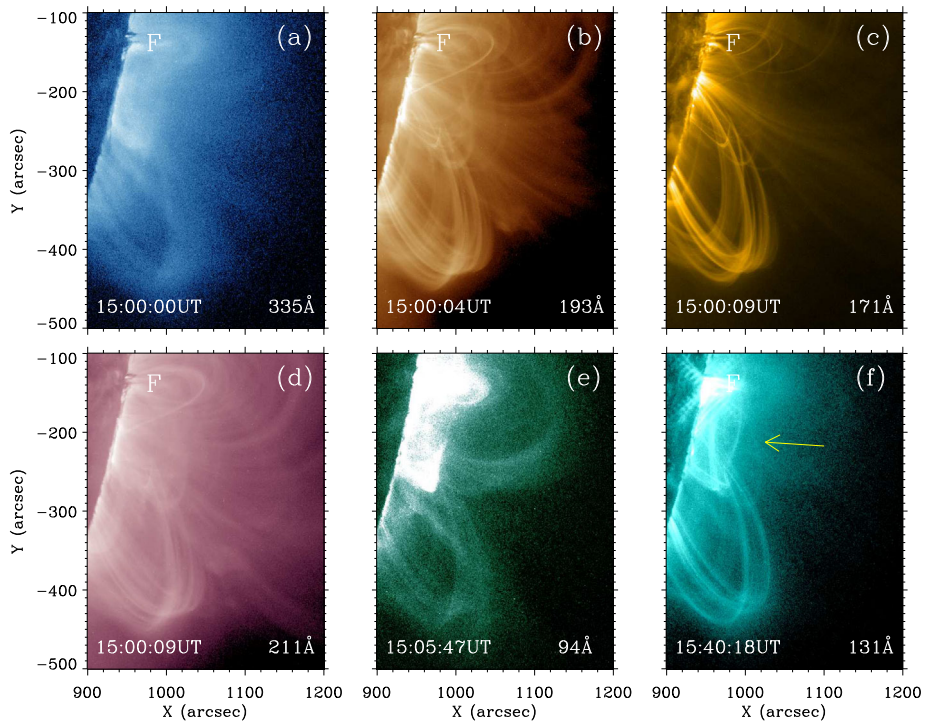


**Figure 2** Observations of coronal loops in different SDO/AIA channels. The yellow arrow in panel f marks a rising flux tube.

region marked by ‘F’, and a plasmoid ejection is found to be rising vertically from it (see Figure 2).

### 3.2. Preflare, Plasmoid Ejections, and the Onset of the Loop Oscillations

Figure 3 shows the normalized flare-intensity profile in the AIA EUV 171-Å data from the flare site ‘F’ (marked by a small box in Figure 1b) and the normalized integrated GOES soft X-ray fluxes in the wavelength bands 0.5–4.0 Å. The AIA intensity curve shows two peaks, one at 15:45:33 UT and the other at 16:07:21 UT. The first peak corresponds to a small flare (say preflare) and the second corresponds to a large flare X8.2 (say main flare). In AIA 171 Å, the preflare started at 15:39 UT and ended at 15:50 UT. However, the preflare emissions are not observed in the GOES X-ray flux profile. The main-flare intensity enhances in the AIA 171 Å just after the preflare, while in GOES X-rays started at 15:45 UT, i.e., during the preflare seen in the AIA 171-Å data. The main-flare peak time in GOES occurs at 16:03:17 UT, i.e., ≈5 minutes before the peak timing of the flare in AIA 171-Å data. The main-flare intensity in AIA 171-Å data ended nearly at 23:00 UT, i.e., it lasted for several hours (≈ 7 hours), while it decayed much faster in GOES X-rays. The long decay phase in AIA 171-Å emissions is caused by heating of the coronal loops at higher altitudes above the flare site (see Figure 4i).

For a detailed analysis of the activity-associated changes in the magnetic field configuration, we have plotted a sample of AIA 171-Å intensity images in Figure 4. This shows the rising of a plasmoid, bending of flux tubes, and occurrence of the main flare. In AIA

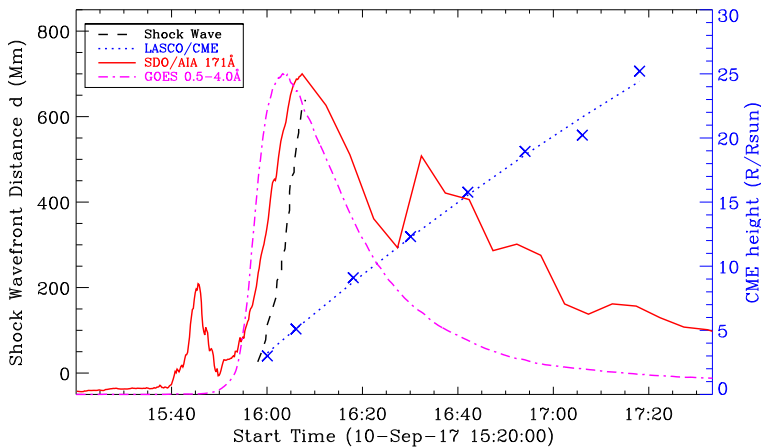


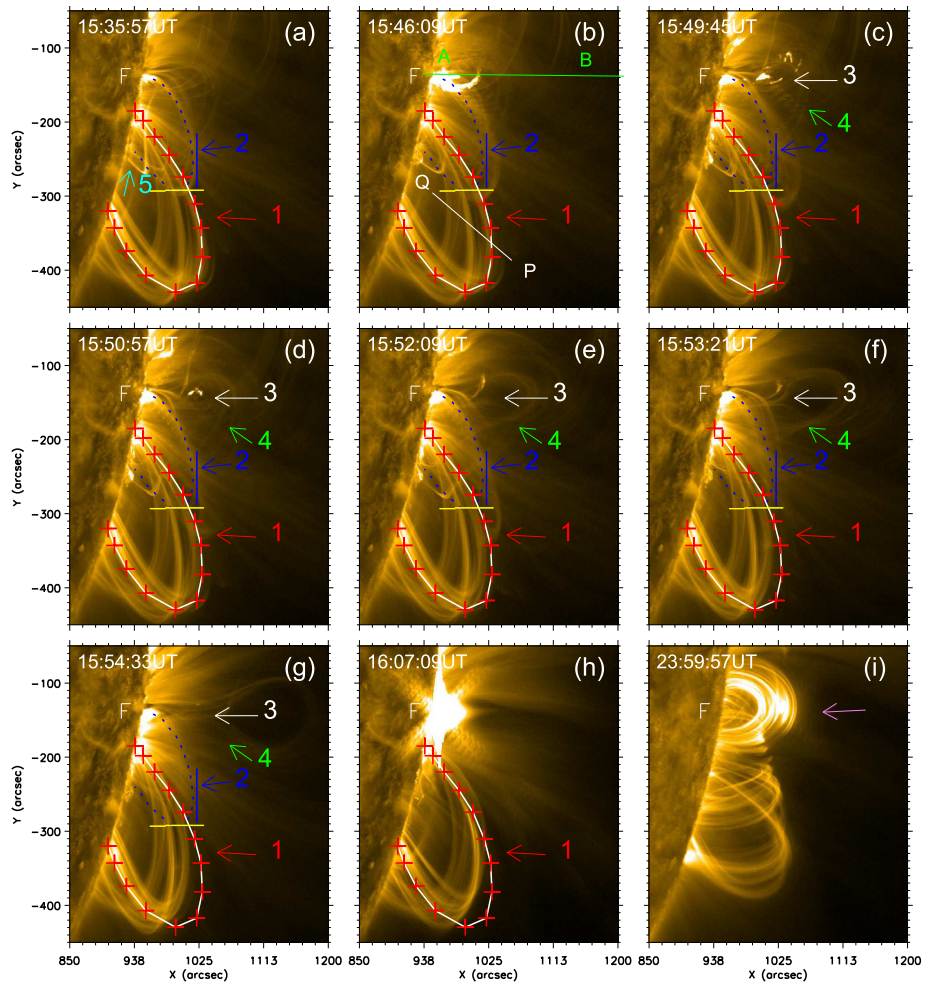
**Figure 3** Relationship between flare-induced shocks and associated CME. The dashed black curve shows the shock-wave front position along the slit ‘6’ direction (see Figure 7a). The ‘+’ symbols mark the CME height from the solar surface and the dotted blue curve represents the quadratic fit. The normalized profiles of SDO/AIA 171-Å intensity (solid red curve) and GOES X-ray flux (dashed-dotted magenta) are plotted for reference.

131-Å data (see Figure 2f), we observed that a magnetic flux rope started rising at 15:40:18 UT and underwent an impulsive acceleration phase around at 15:46:56 UT. However, in the AIA 171-Å intensity images, we observed a magnetic flux rope (MFR) associated with the preflare that rose at 15:49:45 UT accompanied by a filament. It grew rapidly and triggered a fast eruption. That is, we only observed the acceleration phase of the MFR in the AIA 171-Å intensity images. During the preflare time, one of the footpoints of a small loop, labeled with number ‘2’, that was in the flare site started to expand southward at 15:41:21 UT.

At flare site ‘F’, we also found a small C1-class flare at 15:23:21 UT that triggered small oscillations in the coronal loop marked by number ‘5’ (Figure 4a) at 15:31:45 UT. This loop detached from the footpoint at 15:37:45 UT and disappeared from the flare site at 15:39:33 UT. Thereafter, the preflare brightening was observed. It seemed that the preflare triggered magnetic reconnection in other field lines that led to the main flare at 15:52:09 UT.

To understand the relation between the energetic activity and the oscillations of coronal loops, we computed the space–time intensity maps along the reference lines AB and QP (see Figure 4b) that are shown in Figure 5. The top panel shows the energetic phenomena such as a flare, a plasmoid ejection, etc. The bottom panel shows the perturbation in loops that triggered the transverse oscillations. During the end phase of the preflare brightening, the plasma at higher altitude seemed to be heated by the flare energy. This might also be due to reconnection of the field lines at the higher atmosphere that resulted in the main initiation. The preflare brightening at higher altitude disappeared at around 15:52 UT and an upward-moving plasmoid was observed from the flare-site ‘F’ at 15:49:45 UT (marked by arrow ‘3’ in Figure 4). The plasmoid was ejected at around 15:56 UT and pushed the field lines downward. Figures 4 and 5a show that some flux tubes were rising during the plasmoid ejection.

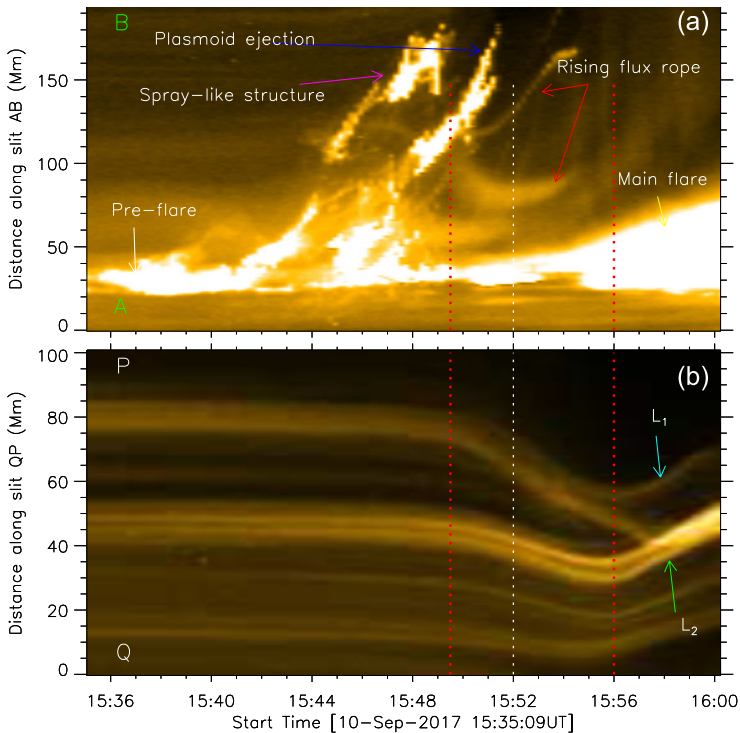
We think that the momentum transfer from the ejected plasmoid pushed the top part of loop ‘2’ towards the solar disk (see Figure 4c). Then, the bent loop ‘2’ pushed loop ‘1’ downwards, till around at 15:56 UT, from its equilibrium position before its eruption. It is also evident from Figure 5 that the bending of the coronal loops happened during the rising



**Figure 4** Images of SDO/AIA 171-Å intensity of the solar atmosphere covering the active region coronal loops. The flare position is marked by the letter ‘F’. Arrow ‘5’ marks a flux tube that erupted before the preflare brightening. The white solid curve with red crosses labeled with number ‘1’ represents a coronal loop (at 15:00:00 UT) that is used for the oscillation studies. The green line AB in panel b illustrates the reference line along which a space–time map, associated with the plasmoid ejection (marked by the arrow 3), is computed and shown in Figure 5a. Similarly, the solid line QP represents the reference position for analyzing the transverse oscillations of coronal loops (see Figure 5b). The blue dotted curve (marked by arrow ‘2’) in panels, a–g, represents the position of the coronal loop (at 15:00:00 UT) concerning the reference position marked by the horizontal (yellow) and the vertical (blue) lines. Green arrow ‘4’ marks a rising flux tube. The violet arrow in panel i shows a system of postflare loops and their brightening at higher altitudes during the decay phase of the main flare.

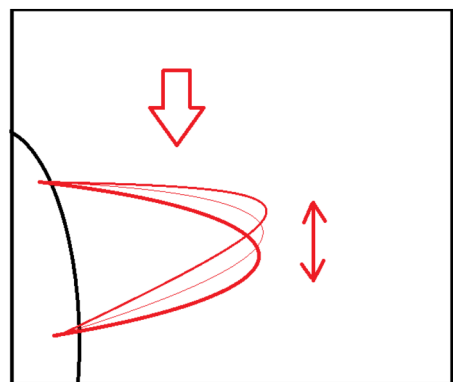
time of the plasmoid from a nearby northern region. We propose that the perturbation by the ejected plasmoid excited the transverse oscillations in the coronal loops.

Figure 6 illustrates the oscillations in the coronal loops. We think that the magnetic pressure force increased in loop ‘1’ due to the suppression from the top of the loop, which is marked with a red arrow. Then, the restoring magnetic tension came into action to reduce



**Figure 5** Association of the plasmoid ejection and the onset of loop oscillations. **(a)** Space-time map of the SDO/AIA 171-Å intensity along the slit AB (see Figure 4b). **(b)** Similar to panel a but along the slit QP (see Figure 4b). The vertical lines mark the timing of the plasmoid rising start, the beginning of the main flare, and the maximum perturbation of coronal loops (from the left to the right). In the bottom panel arrows  $L_1$  and  $L_2$  mark the positions of the two coronal loops considered for the oscillation studies.

**Figure 6** Transverse oscillations of the coronal loop '1' (see Figure 4), where red up and down arrows represent the oscillating direction. The red arrow pointing towards down shows that the perturbation comes from the top of the loop.



the excess pressure force by moving loop '1' upward and initiated oscillations in the loops. The loops are subjected to kink oscillations but they appear to be moving radially up and down due to projection effects.



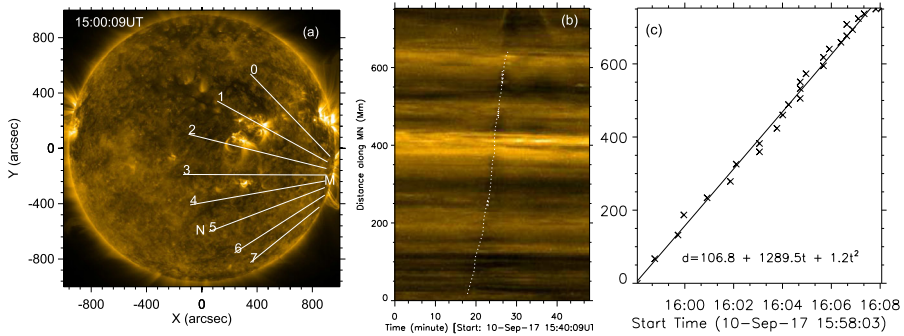


**Figure 7** (a) Full disk AIA 171-Å intensity map, where numbered *white solid lines* mark the slit positions for shock-wave analysis. (b) The space–time intensity map along the slit 6, where the overlying *white dashed curve* represents the shock-front position. (c) Least-squares quadratic fit to the shock-front position as shown in the panel b.

### 3.3. Shock Waves and Coronal Mass Ejections

We observed a shock wave propagating away from the flare site. It propagated mostly southward with part of it reflecting towards the north. To study the propagation of shock waves across the disk and their role in the triggering of loop oscillations, we considered eight slits along the direction of their propagation from the point of their initiation (see Figure 7a). Further, to illustrate the wave propagation, we constructed a space–time intensity map along the slit 6 as the wave is seen in the bottom part of the solar disk in Figure 7a. Thus, the computed shock-wave map is shown in Figure 7b. The overlying white dashed curve marks the wavefront position. The shock wave starts around at 15:58 UT along slit 6 direction. We calculated the shock-wave propagating speed along the slit 6 from the space–time map using a quadratic fit to the wavefront positions as shown in the right panel c. We found the speed of the shock wave to be  $\approx 1290 \text{ km s}^{-1}$  with an acceleration of  $\approx 1.2 \text{ km s}^{-2}$ .

We found that the shock wave first appeared at 15:54:00 UT during the impulsive phase of the main flare and increased its velocity during its propagation (also reported by Gopalswamy et al., 2018). However, the coronal loops were already perturbed by the ejected plasmoid at 15:49:45 UT before the arrival of the shock wave. Therefore, we think that the shock wave did not trigger the loop oscillations.

The SOHO/LASCO observations showed a halo CME associated with the main flare (see Figure 8), which first appeared around 16:00 UT in C2 field of view (panel a), having a position angle of  $263^\circ$  and angular width of  $360^\circ$ . This CME is found to be moving with a speed of  $3693 \text{ km s}^{-1}$  and a deceleration of  $-116 \text{ m s}^{-2}$  (see Figure 3). Gopalswamy et al. (2018) found that this CME was one of the most intense and energetic eruptions in the SOHO era with ground-level enhancement (GLE) and solar energetic particle (SEP) events.

The relationships between the flare, CME, and the shock-wave occurrence are shown in Figure 3. The CME appeared first at nearly 16:00 UT, i.e., along with the shock wave and after a few minutes of the start of the main flare seen in AIA 171-Å and GOES X-ray fluxes. The impulsive acceleration phase of the CME merged with the rising phase of the main flare while, in the propagation phase, the CME speed increased.

### 3.4. Transverse Oscillations of Coronal Loops

To analyze the properties of the transverse oscillations of coronal loops, we identified distinct loops in the AIA 171-Å intensity images and selected two oscillating loops named as

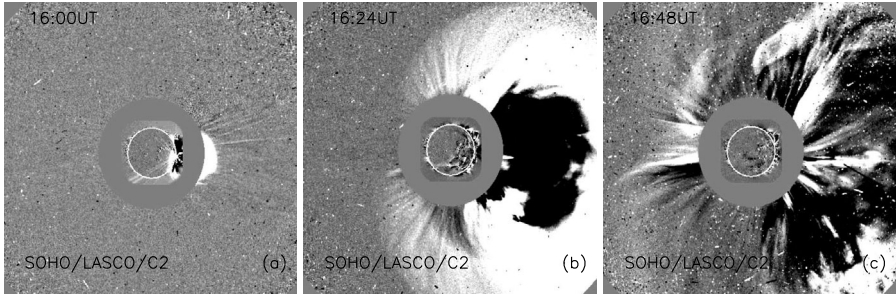
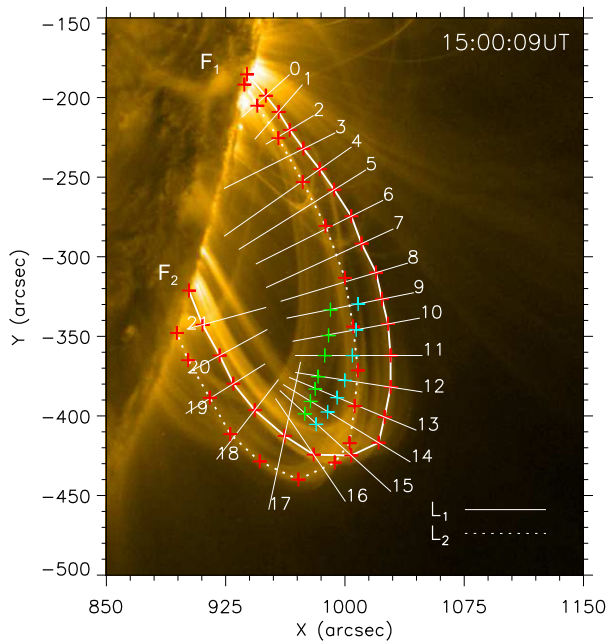


**Figure 8** Intensity images of the Sun observed by SDO/AIA and SOHO/LASCO-C2 during the start (a), peak (b), and propagation (c) times of the CME associated with the X8.2.

**Figure 9** An SDO/AIA 171-Å intensity image overlaid with marked coronal loops  $L_1$  (solid curve) and  $L_2$  (dashed curve) at 15:00:10 UT.  $F_1$  and  $F_2$  correspond to the footpoints of the coronal loops. The line segments 0–21 mark the slit positions perpendicular to the loop  $L_1$  that are used to compute the space–time intensity maps as shown in Figure 10. The cyan and green points represent the positions of loops  $L_1$  and  $L_2$ , respectively, at 15:56:10 UT.



$L_1$  and  $L_2$  (see Figure 9) with sufficient quality for time-series analysis. Further, to find the changes in the loop position as functions of space and time, we took 22 slits across the loops, as shown in Figure 9. Then, space–time intensity maps for all slits were computed by combining the intensity values along different slits as a function of time. Thus, the space–time intensity maps for the seven chosen positions are shown in Figure 10. The amplitude of loop oscillations across all the slits and for all the loops decreases with time. We searched for clear oscillatory patterns in coronal loops by analyzing the space–time maps where at least three to four cycles of loop oscillations were seen. Thus, we considered two loops marked by  $L_1$  and  $L_2$  as shown in the space–time map for the slit number 10.

The time series of the loop displacements were extracted from the space–time maps by following the loop intensity as a function of time. To obtain the position of a loop more accurately, first we manually found its location from the space–time map by following the intensity of the loop. We repeated this procedure ten times for a loop in a given slit. Then,

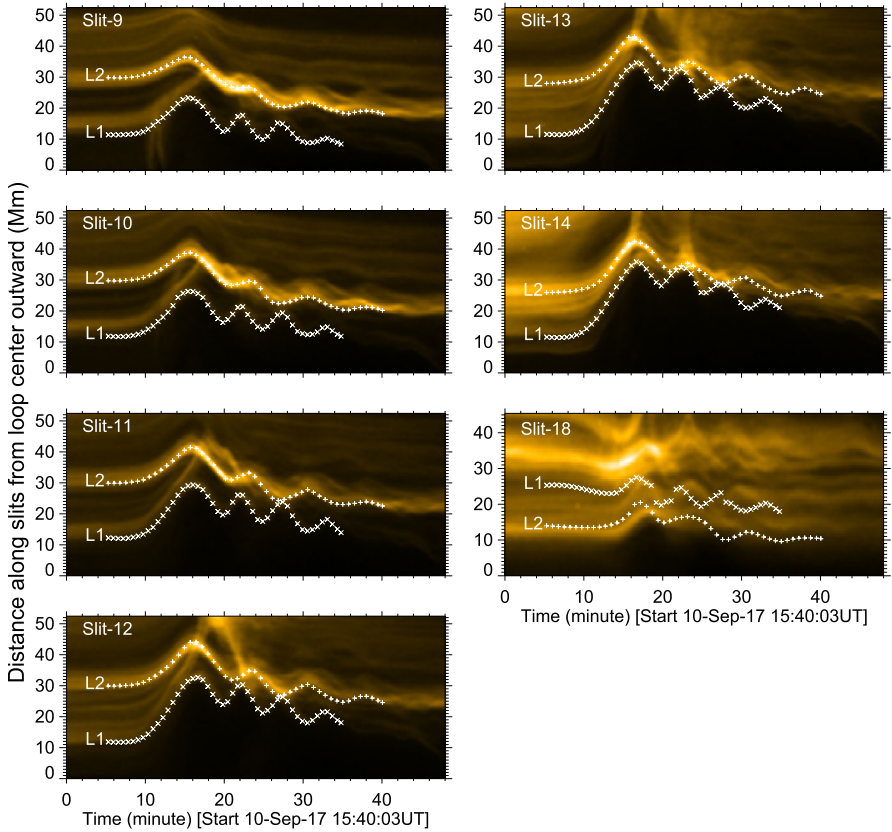


**Figure 10** Space–time maps of AIA 171-Å intensity along ten different slit positions (slits 9–14, 18) across the  $L_1$  and  $L_2$  loops as shown in Figure 9. The overlaid crosses (‘×’) and plus (‘+’) symbols mark the positions of the loops,  $L_1$  and  $L_2$ .

their mean and the standard deviation were taken as the loop positions and errors. Earlier researchers have adopted similar methods for the studies of transverse oscillations of coronal loops (e.g., Jain, Maurya, and Hindman, 2015; Nechaeva et al., 2019). In Figure 10, the mean positions of both loops for different slits are overlaid with cross and plus symbols.

Further, to show the oscillation properties of loops, the mean positions of loops as a function of time are plotted in the top panel of Figure 11 for the loop  $L_1$  (left) and  $L_2$  (right). The time, 15:56:45 UT, of the maximum displacement of the loops from their equilibrium positions, is considered as the reference time for the oscillation studies. To find the oscillation properties in the loops, we subtracted a linear trend for  $L_1$  and a quadratic trend for  $L_2$  from the time series, and the final time series is shown in the middle panels of Figure 11. We determined the oscillation parameters by fitting an exponential damping cosine function of the form,

$$d(t) = A \cos\left(\frac{2\pi t}{P} + \phi\right) e^{-t/\tau}, \tag{1}$$

where,  $A$  is the amplitude,  $\tau$  is the damping time,  $P$  is the period of oscillation and  $\phi$  is the phase. This fitting is performed by Levenberg–Marquardt least-squares minimization using

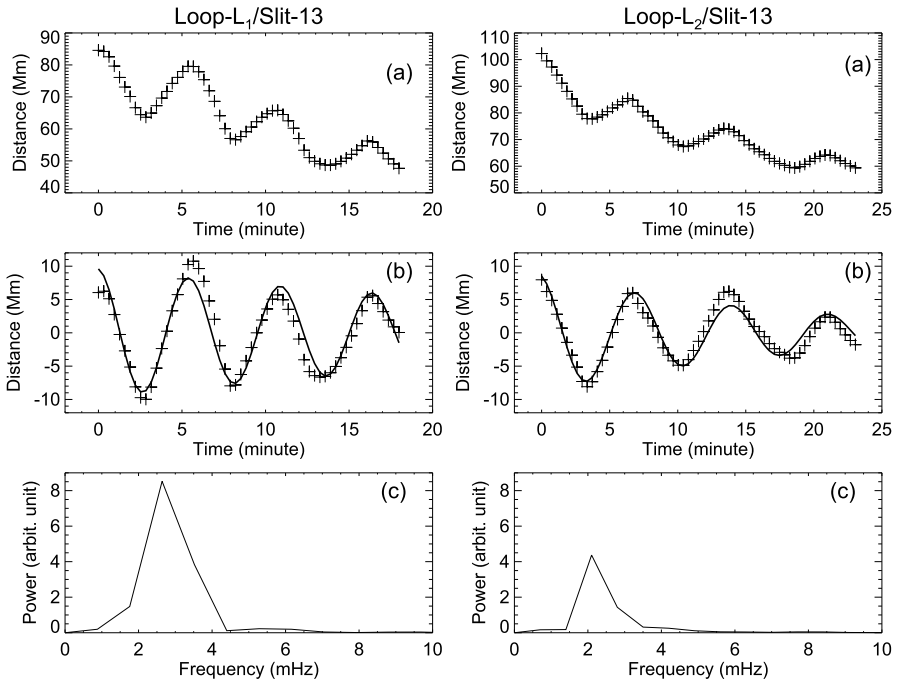


**Figure 11** Transverse oscillations of coronal loops  $L_1$  (left) and  $L_2$  (right) across the slit 13. *Top row:* The crosses correspond to the loop positions estimated from the space–time maps. *Middle row:* Time series of the loop positions after subtracting a low-degree polynomial. The *solid curve* represents the damp fit Equation 1. *Bottom row:* Fourier power spectra of the time series shown in the middle panel.

**Table 1** Oscillation parameters of the coronal loop  $L_1$  along different slit positions.

Slit No.	Amplitude (Mm)	Period from damp fitting $P_1$ (minute)	Damping time $\tau$ (minute)	Period from power spectra $P_2$ (minute)
9	$30 \pm 1$	$5.40 \pm 0.01$	$16.1 \pm 0.5$	6.31
10	$18.0 \pm 0.9$	$5.35 \pm 0.01$	$26 \pm 1$	6.31
11	$12.6 \pm 0.4$	$5.41 \pm 0.01$	$56 \pm 4$	6.31
12	$11.5 \pm 0.3$	$5.43 \pm 0.01$	$68 \pm 5$	6.31
13	$15.7 \pm 0.6$	$5.49 \pm 0.01$	$34 \pm 1$	6.31
14	$21.5 \pm 0.8$	$5.56 \pm 0.01$	$22.0 \pm 0.6$	6.31
18	$23.4 \pm 0.8$	$5.28 \pm 0.01$	$16.7 \pm 0.4$	6.31

the MPFITFUN (Markwardt, 2009) in the Interactive Data Language (IDL). We find that the damp fit does not precisely fit the loop positions. Therefore, to estimate more accurately the oscillation period, we compute the Fourier power spectra of the loop oscillation time series as shown in the bottom panel of Figure 11. We repeated this calculation for the seven slit positions (9 to 14 and 18) for both the loops  $L_1$  and  $L_2$ . The oscillation parameters obtained from the fits and the Fourier spectra are listed in Tables 1 and 2 for the loops  $L_1$  and  $L_2$ , respectively.

**Table 2** Oscillation parameters of the loop  $L_2$  along different slit positions.

Slit No.	Amplitude (Mm)	Period from damp fitting $P_1$ (minute)	Damping time $\tau$ (minute)	Period from power spectra $P_2$ (minute)
9	$7.0 \pm 0.5$	$7.13 \pm 0.02$	$28 \pm 2$	7.93
10	$18.7 \pm 0.8$	$7.10 \pm 0.01$	$17.6 \pm 0.5$	7.93
11	$19.7 \pm 0.7$	$7.11 \pm 0.01$	$19.1 \pm 0.5$	7.93
12	$23.0 \pm 0.7$	$6.85 \pm 0.01$	$18.8 \pm 0.4$	7.93
13	$21.7 \pm 0.7$	$7.10 \pm 0.01$	$18.6 \pm 0.4$	7.93
14	$20.0 \pm 0.7$	$7.50 \pm 0.01$	$20.0 \pm 0.4$	7.93
18	$30 \pm 2$	$7.69 \pm 0.03$	$12.4 \pm 0.4$	7.93

From the damp fittings, we find that the loop  $L_2$  oscillates with a significantly larger period than the loop  $L_1$  but with a shorter damping time and comparable amplitudes. Small deviations in the periods from different cuts could be mainly due to the estimated position of loops in the space–time intensity maps. However, from the Fourier power spectra of the oscillation time series, we obtained the same period of oscillations for different cuts of a given loop. We think that the single peak in the power spectra of both loops provides evidence that the oscillations are in the fundamental mode.

Further, to confirm the fundamental mode of oscillations in a coronal loop, we analyzed the cross-spectra and the crossphases in different time series obtained from different slits for the same loop (see Figure 12). The point of intersection between a line from the peak of the cross-spectrum and curve of the phase spectrum is taken as the phase difference of two points along the loop. The phase differences along the loop between slits determine whether the oscillations are in phase. We did not find any significant phase difference for the slit positions of a loop. This confirms that both loops are oscillating in the fundamental modes.

We estimated the kink speed, Alfvén speed, and the magnetic field by finding the loop length and the period of oscillations. The length of a coronal loop can be estimated more accurately by comparing its observations from two different viewpoints, e.g., using one observation from the *Extreme Ultraviolet Imager (EUVI)/Solar Terrestrial Relations Observatory (STEREO)* and the other from SDO/AIA, or both from STEREO A and B (Aschwanden and Schrijver, 2011; Verwichte et al., 2013; White and Verwichte, 2012). This method gives a more accurate length of the loop instead of a projected image on the plane of sky. However, for this event, the oscillating loops are only seen in SDO/AIA and not in the STEREO/EUVI channels. Therefore, we cannot estimate the 3D loop geometry using the above approach. To find the loop length, first, we identified the footpoints at an earlier time (on 10 September 2017 at 00:15:10 UT) when they were clearly visible on the solar disk. Then, using the locations of the loops just before the oscillations and the footpoints, we estimated the loop lengths as discussed by Aschwanden et al. (2002). The projection effect mainly causes the errors on the loop-length measurements. Thus, the estimated lengths of the coronal loops are listed in Table 3. Previous studies showed that the periods of oscillations are proportional to the length of a loop (e.g., Goddard and Nakariakov, 2016). However, we find that the smaller loop  $L_2$  oscillates with a more extended period than the loop  $L_1$ . This could be due to an error in the measurements of the loop lengths.

For a fundamental mode of oscillation, the longitudinal phase speed can be expressed in terms of the period of the kink oscillation ( $P$ ) and the loop length (Roberts, Edwin, and

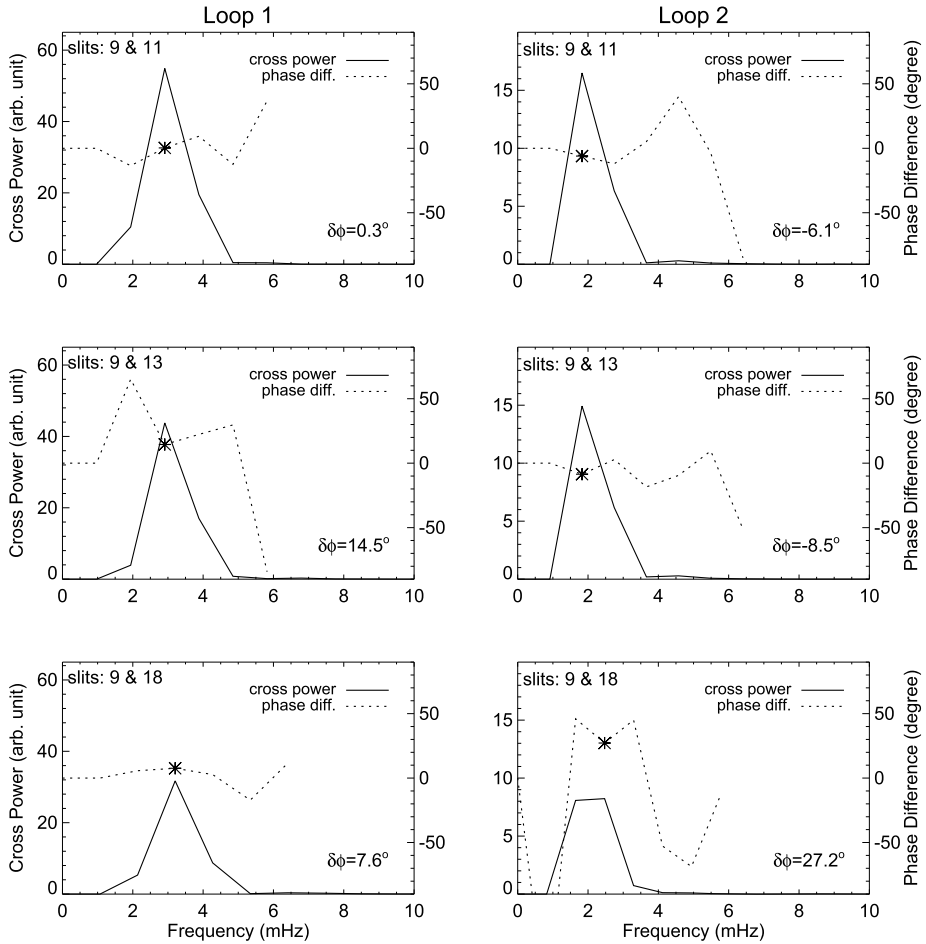


**Figure 12** Crosspower spectra (*solid curve*) and phase difference (*dotted curve*) profiles obtained from times series of the loop oscillations across the slits 8 and 11 (*top row*), 8 and 13 (*middle row*), and 8 and 18 (*bottom row*) for the coronal loops  $L_1$  (*left column*) and  $L_2$  (*right column*). For positions of the slits, see Figure 9. The *asterisks symbol* \* on the phase profile marks the phase difference ( $\delta\phi$ ) between two time series.

Benz 1984; Verwichte et al. 2009),

$$V_{ph} = \frac{2L}{P}. \tag{2}$$

Further, from the MHD wave theory, the fast-kink standing waves are strongly dispersive with real wave number and frequency. The phase speed of a fast-kink mode, in the long wavelength ( $k \ll 1$ ) and zero plasma- $\beta$  limit, equals the kink speed  $C_k$  (Edwin and Roberts, 1983). In the thin-tube approximation of kink-mode oscillations,  $C_k$  can also be represented (Roberts, Edwin, and Benz, 1984) as,

$$C_k = V_{A0} \sqrt{\frac{2}{1 + \rho_{ex}/\rho_{in}}}, \tag{3}$$

**Table 3** Oscillation parameters, the magnetic field values, and the Alfvén speed in the coronal loops.

Loop	Period $P$ (minute)	Length (Mm)	Kink speed ( $\text{km s}^{-1}$ )	Alfvén speed ( $\text{km s}^{-1}$ )	Magnetic field (G)
$L_1$	6.31	195	1029	763	36
$L_2$	7.93	199	836	620	29

which is related to the internal Alfvén speed  $V_{A0}$  and the internal ( $\rho_{in}$ ) and external ( $\rho_{ex}$ ) plasma densities of the loop. The Alfvén speed is defined in terms of the magnetic field and the density of the loop. Considering a uniform magnetic field and Equation 3, the kink speed can be written as,

$$C_k = B \sqrt{\frac{2}{\mu_0(\rho_{in} + \rho_{ex})}}, \tag{4}$$

where,  $B$  is the magnetic field strength in the loop and  $\mu_0$  is the permeability of free space. Assuming that the density ratio is  $\rho_{ex}/\rho_{in} \approx 0.1$  (Nakariakov et al., 1999), the Alfvén speed ranges between,

$$\frac{2L}{\sqrt{2}P} \leq V_{A0} \leq \frac{2L}{P}, \tag{5}$$

and hence the magnetic field in the coronal loop can be expressed as

$$B = V_{A0} \sqrt{\mu_0 \mu_c m_p n_e}, \tag{6}$$

where,  $\mu_c = 1.27$  is the mean molecular weight in the corona and  $m_p$  is the proton mass. The electron density  $n_e$  in the coronal plasma can be taken as  $(7-10) \times 10^9 \text{ cm}^{-3}$  (Sun et al., 2013). Then, the magnetic field range can be expressed (Verwichte et al., 2009; White and Verwichte, 2012; Nakariakov and Ofman, 2001) as

$$\frac{2L}{\sqrt{2}P} \sqrt{\mu_0 \mu_c m_p n_e} \leq B \leq \frac{2L}{P} \sqrt{\mu_0 \mu_c m_p n_e}. \tag{7}$$

Using the previous equations, and the oscillation properties of the coronal loops, we can estimate the Alfvén speed and the magnetic field in the coronal loops. Thus, computed values for the two loops are listed in Table 3. The values of the magnetic field in the coronal loops seem to be reasonable.

The seismological determination carried out above yields a single average value for the kink speed and the magnetic field for the loop. In fact, the density and magnetic field vary continuously along the loop. One can estimate these parameters along the loops using other methods such as magnetic field extrapolation and spectral information from the SDO/AIA passbands (e.g., Verwichte et al., 2013). Therefore, the average parameters obtained from the coronal seismology may differ from the parameters along the loop. This discrepancy was reported initially by Aschwanden and Schrijver (2011) and others (such as, Verwichte et al., 2013).

#### 4. Summary and Conclusions

Using the EUV-intensity observations of the solar corona, we analyzed the transverse oscillations in the coronal loops of an active region that was located at the west limb of the solar

disk. The active region was found to be a complex area with mixed magnetic polarities. One footpoint of the coronal loops was found to be anchored in the active-region center and the other in the nearby diffused-polarity regions

The initiation of the loop oscillations is found to be triggered by a plasmoid eruption followed by a preflare that initiated reconnection of field lines leading to a large X8.2 class flare. During the preflare, a flux rope was found to be rising slowly then expanding and finally undergoing an acceleration phase. The magnetic field lines seemed to reconnect during its expansion phase and a flare brightening was observed. This flux rope was found to be associated with the formation of a plasmoid. During the ejection of the plasmoid, the coronal loop interacted with the nearby loops and initiated an oscillation before the main impulsive phase of the flare. We analyzed the oscillation properties in two distinct coronal loops and computed the coronal magnetic fields.

We found that the loops oscillated with average periods of 6.31 minutes and 7.93 minutes, with average damping times of  $\approx 34$  minutes and  $\approx 19$  minutes, respectively. In the Fourier power spectra of the loop oscillation, we found a single peak that showed the oscillation to be in the fundamental mode. Further, from the phase analysis between two successive slit directions along a single loop, we confirmed that different parts of the loop oscillated in the same phase. The length of the loops turned out to be  $L_1 = 195$  Mm and  $L_2 = 199$  Mm. Generally, the period of oscillation is proportional to the length of the oscillating loop, average loop magnetic field strength, and square-root of the mass density (Aschwanden and Boerner, 2011). Using the period of oscillations and loop lengths, we estimated the kink speed, Alfvén speed, and hence the magnetic field associated with the oscillating loops. Thus, the estimated magnetic fields in the coronal loops are found to be  $\approx 36$  G and  $\approx 29$  G, respectively.

We observed a flare-induced shock wave propagating across the solar disk with an average speed of  $1290 \text{ km s}^{-1}$  and an acceleration of about  $1.2 \text{ km s}^{-2}$ . These waves covered the entire solar disk and also touched on the upper atmospheric layers. Initially, they traveled towards the southern polar regions and reflected on the disk. Other researchers have also reported earlier (Seaton and Darnel, 2018; Liu et al., 2018) that this is the first observation of a truly global EUV wave with SDO/AIA observations. From the SOHO/LASCO CME catalog, we also found that the main flare was accompanied by a fast-propagating halo CME. Gopalswamy et al. (2018) reported that this CME was the most intense eruption in the SOHO era accompanied by a ground-level enhancement (GLE) and a solar energetic particle (SEP) event. We found that the flare-generated shocks and the associated CME started during the impulsive phase of the main flare.

There are three possible sources of the perturbations that lead to the oscillations in the coronal loops: (1) the rising plasmoid increased in size due to a reduction of density and pushed the coronal-loop field lines from their equilibrium positions, (2) during the preflare time, a risen flux tube pushed down the loops from their equilibrium, and (3) the shock wave generated at the time of the plasmoid ejection. From a careful analysis of the time sequence of these events, we concluded that the plasmoid eruption caused the oscillations in the loops. It would be interesting to analyze these events on the solar disk and compare the magnetic field obtained from other methods such as extrapolations.

**Acknowledgments** This work uses the observational data obtained from the SDO/AIA, HMI and SOHO/LASCO. SOHO is a project of international collaboration between ESA and NASA. The integrated X-ray flux data were obtained from GOES, operated by the National Oceanic and Atmospheric Administration, USA. We thank the referee for his/her valuable comments and suggestions that helped us to improve the manuscript. We thank Durgesh Tripathi of IUCAA for his valuable comments and suggestions that helped us to improve the manuscript. R.A.M. thankfully acknowledges the support by the NITC/FRG-2019 under which this work was carried out.



**Author contributions** Safna Banu K. analyzed the observational data and drafted the manuscript. Jain Jacob P.T. helped in analyzing the data, reviewed the manuscript. R.A. Maurya guided the research work and edited the manuscript.

**Data Availability** The datasets analyzed during the current study are available in the Joint Science Operations Center (JSOC) repository, <http://jsoc.stanford.edu/>.

## Declarations

**Disclosure of Potential Conflicts of Interest** The authors declare that they have no conflicts of interest.

**Competing interests** The authors declare no competing interests.

## References

- Anfinogentov, S., Nisticò, G., Nakariakov, V.M.: 2013, Decay-less kink oscillations in coronal loops. *Astron. Astrophys.* **560**, A107. [DOI](#).
- Aschwanden, M.J., Boerner, P.: 2011, Solar coronal loop studies with the atmospheric imaging assembly. I. Cross-sectional temperature structure. *Astrophys. J.* **732**(2), 81. [DOI](#).
- Aschwanden, M.J., Schrijver, C.J.: 2011, Coronal loop oscillations observed with atmospheric imaging assembly—kink mode with cross-sectional and density oscillations. *Astrophys. J.* **736**(2), 102. [DOI](#).
- Aschwanden, M.J., Terradas, J.: 2008, The effect of radiative cooling on coronal loop oscillations. *Astrophys. J.* **686**(2), L127. [DOI](#). [ADS](#).
- Aschwanden, M.J., Fletcher, L., Schrijver, C.J., Alexander, D.: 1999, Coronal loop oscillations observed with the transition region and coronal explorer. *Astrophys. J.* **520**(2), 880. [DOI](#).
- Aschwanden, M.J., Pontieu, B.D., Schrijver, C.J., Title, A.M.: 2002, Transverse oscillations in coronal loops observed with TRACE II. Measurements of geometric and physical parameters. *Solar Phys.* **206****206**(11), 99. [DOI](#).
- Brosius, J.W., Davila, J.M., Thomas, R.J., White, S.M.: 1997, Coronal magnetography of a solar active region using coordinated SERTS and VLA observations. In: *AAS/Solar Phys. Div. Meeting* **28**, 01.35. [ADS](#).
- Brueckner, G.E., Howard, R.A., Koomen, M.J., Korendyke, C.M., Michels, D.J., Moses, J.D., Socker, D.G., Dere, K.P., Lamy, P.L., Llebaria, A., Bout, M.V., Schwenn, R., Simnett, G.M., Bedford, D.K., Eyles, C.J.: 1995, The Large Angle Spectroscopic Coronagraph (LASCO). *Solar Phys.* **162**(1–2), 357. [DOI](#).
- Doorselaere, T.V., Nakariakov, V.M., Verwichte, E.: 2007, Coronal loop seismology using multiple transverse loop oscillation harmonics. *Astron. Astrophys.* **473**(3), 959. [DOI](#).
- Edwin, P.M., Roberts, B.: 1983, Wave propagation in a magnetic cylinder. *Solar Phys.* **88**(1–2), 179. [DOI](#).
- Gelfreikh, G.B.: 1999, Physics of the solar active regions from radio observations. In: Bastian, T.S., Gopalswamy, N., Shibasaki, K. (eds.) *Proc. Nobeyama Symp.*, 41. [ADS](#).
- Goddard, C.R., Nakariakov, V.M.: 2016, Dependence of kink oscillation damping on the amplitude. *Astron. Astrophys.* **590**, L5. [DOI](#).
- Goddard, C.R., Nisticò, G., Nakariakov, V.M., Zimovets, I.V.: 2016, A statistical study of decaying kink oscillations detected using SDO/AIA. *Astron. Astrophys.* **585**, A137. [DOI](#).
- Goossens, M., Andries, J., Aschwanden, M.J.: 2002, Coronal loop oscillations. *Astron. Astrophys.* **394**(3), L39. [DOI](#).
- Gopalswamy, N., Yashiro, S., Mäkelä, P., Xie, H., Akiyama, S., Monstein, C.: 2018, Extreme kinematics of the 2017 September 10 solar eruption and the spectral characteristics of the associated energetic particles. *Astrophys. J.* **863**(2), L39. [DOI](#).
- Hollweg, J.V., Yang, G.: 1988, Resonance absorption of compressible magnetohydrodynamic waves at thin “surfaces”. *J. Geophys. Res.* **93**(A6), 5423. [DOI](#).
- Hudson, H.S., Warmuth, A.: 2004, Coronal loop oscillations and flare shock waves. *Astrophys. J. Lett.* **614**, L85. [DOI](#). [ADS](#).
- Jain, R., Maurya, R.A., Hindman, B.W.: 2015, Fundamental-mode oscillations of two coronal loops within a solar magnetic arcade. *Astrophys. J.* **804**(1), L19. [DOI](#).
- Lemen, J.R., Title, A.M., Akin, D.J., Boerner, P.F., Chou, C., Drake, J.F., Duncan, D.W., Edwards, C.G., Friedlaender, F.M., Heyman, G.F., Hurlburt, N.E., Katz, N.L., Kushner, G.D., Levay, M., Lindgren, R.W., Mathur, D.P., McFeaters, E.L., Mitchell, S., Rehse, R.A., Schrijver, C.J., Springer, L.A., Stern, R.A., Tarbell, T.D., Wuelsner, J.-P., Wolfson, C.J., Yanari, C., Bookbinder, J.A., Cheimets, P.N., Caldwell, D., Deluca, E.E., Gates, R., Golub, L., Park, S., Podgorski, W.A., Bush, R.I., Scherrer, P.H., Gumm, M.

- M.A., Smith, P., Aufer, G., Jerram, P., Pool, P., Soufli, R., Windt, D.L., Beardsley, S., Clapp, M., Lang, J., Waltham, N.: 2011, The Atmospheric Imaging Assembly (AIA) on the Solar Dynamics Observatory (SDO). *Solar Phys.* **275**(1–2), 17. [DOI](#).
- Liu, W., Jin, M., Downs, C., Ofman, L., Cheung, M.C.M., Nitta, N.V.: 2018, A truly global extreme ultraviolet wave from the SOL2017-09-10 x8.2+ solar flare-coronal mass ejection. *Astrophys. J.* **864**(2), L24. [DOI](#).
- Markwardt, C.B.: 2009, Non-linear least-squares fitting in IDL with MPFIT. In: Bohlender, D.A., Durand, D., Dowler, P. (eds.) *Astronomical Data Analysis Software and Systems XVIII, Astron. Soc. Pacific Conf. Ser.* **411**, 251. [ADS](#).
- McLaughlin, J.A., Ofman, L.: 2008, Three-dimensional magnetohydrodynamic wave behavior in active regions: individual loop density structure. *Astrophys. J.* **682**(2), 1338. [DOI](#).
- Mitra, P.K., Joshi, B.: 2019, Preflare processes, flux rope activation, large-scale eruption, and associated X-class flare from the active region NOAA 11875. *Astrophys. J.* **884**(1), 46. [DOI](#).
- Moortel, I.D., Brady, C.S.: 2007, Observation of higher harmonic coronal loop oscillations. *Astrophys. J.* **664**(2), 1210. [DOI](#).
- Nakariakov, V.M., Ofman, L.: 2001, Determination of the coronal magnetic field by coronal loop oscillations. *Astron. Astrophys.* **372**(3), L53. [DOI](#).
- Nakariakov, V.M., Verwichte, E.: 2005, Coronal waves and oscillations. *Living Rev. Solar Phys.* **2**, 3. [DOI](#).
- Nakariakov, V.M., Ofman, L., DeLuca, E.E., Roberts, B., Davila, J.M.: 1999, TRACE observation of damped coronal loop oscillations: implications for coronal heating. *Science* **285**(5429), 862. [DOI](#).
- Nakariakov, V.M., Anfinogentov, S.A., Antolin, P., Jain, R., Kolotkov, D.Y., Kupriyanova, E.G., Li, D., Magyar, N., Nisticò, G., Pascoe, D.J., Srivastava, A.K., Terradas, J., Vasheghani Farahani, S., Verth, G., Yuan, D., Zimovets, I.V.: 2021, Kink oscillations of coronal loops. *Space Sci. Rev.* **217**(6), 73. [DOI](#). [ADS](#).
- Nechaeva, A., Zimovets, I.V., Nakariakov, V.M., Goddard, C.R.: 2019, Catalog of decaying kink oscillations of coronal loops in the 24th solar cycle. *Astrophys. J. Suppl. Ser.* **241**(2), 31. [DOI](#).
- Nindos, A., Patsourakos, S., Vourlidis, A., Tagikas, C.: 2015, How common are hot magnetic flux ropes in the low solar corona? A statistical study of EUV observations. *Astrophys. J.* **808**(2), 117. [DOI](#).
- Nisticò, G., Nakariakov, V.M., Verwichte, E.: 2013, Decaying and decayless transverse oscillations of a coronal loop. *Astron. Astrophys.* **552**, A57. [DOI](#).
- O'Dwyer, B., Del Zanna, G., Mason, H.E., Weber, M.A., Tripathi, D.: 2010, SDO/AIA response to coronal hole, quiet sun, active region, and flare plasma. *Astron. Astrophys.* **521**, A21. [DOI](#). [ADS](#).
- Ofman, L.: 2009, Progress, challenges, and perspectives of the 3D MHD numerical modeling of oscillations in the solar corona. *Space Sci. Rev.* **149**(1–4), 153. [DOI](#).
- Roberts, B., Edwin, P.M., Benz, A.O.: 1984, On coronal oscillations. *Astrophys. J.* **279**, 857. [DOI](#).
- Ruderman, M.S., Roberts, B.: 2002, The damping of coronal loop oscillations. *Astrophys. J.* **577**(1), 475. [DOI](#). [ADS](#).
- Russell, A.J.B., Simões, P.J.A., Fletcher, L.: 2015, A unified view of coronal loop contraction and oscillation in flares. *Astron. Astrophys.* **581**, A8. [DOI](#).
- Ryabov, B.I., Pilyeva, N.A., Alissandrakis, C.E., Shibasaki, K., Bogod, V.M., Garaimov, V.I., Gelfreikh, G.B.: 1999, Coronal magnetography of an active region from microwave polarization inversion. *Solar Phys.* **185**(1), 157. [DOI](#). [ADS](#).
- Ryabov, B.I., Maksimov, V.P., Lesovoi, S.V., Shibasaki, K., Nindos, A., Pevtsov, A.: 2005, Coronal magnetography of solar active region 8365 with the SSRT and NoRH radio heliographs. *Solar Phys.* **226**(2), 223. [DOI](#). [ADS](#).
- Seaton, D.B., Darnel, J.M.: 2018, Observations of an eruptive solar flare in the extended EUV solar corona. *Astrophys. J.* **852**(1), L9. [DOI](#).
- Shibata, K.: 1996, New observational facts about solar flares from YOHKOH studies — evidence of magnetic reconnection and a unified model of flares. *Adv. Space Res.* **17**(4–5), 9. [DOI](#).
- Sun, X., Hoeksema, J.T., Liu, Y., Aulanier, G., Su, Y., Hannah, I.G., Hock, R.A.: 2013, Hot spline loops and the nature of a late-phase solar flare. *Astrophys. J.* **778**(2), 139. [DOI](#).
- Verwichte, E., Aschwanden, M.J., Doorsselaere, T.V., Foullon, C., Nakariakov, V.M.: 2009, Seismology of a large solar coronal loop from EUVI/STEREO observations of its transverse oscillation. *Astrophys. J.* **698**(1), 397. [DOI](#).
- Verwichte, E., Doorsselaere, T.V., Foullon, C., White, R.S.: 2013, Coronal Alfvén speed determination: consistency between seismology using AIA/SDO transverse loop oscillations and magnetic extrapolation. *Astrophys. J.* **767**(1), 16. [DOI](#).
- Wang, T., Ofman, L., Davila, J.M., Su, Y.: 2012, Growing transverse oscillations of a multistranded loop observed by SDO/AIA. *Astrophys. J.* **751**, L27.
- White, R.S., Verwichte, E.: 2012, Transverse coronal loop oscillations seen in unprecedented detail by AIA/SDO. *Astron. Astrophys.* **537**, A49. [DOI](#).

- White, R.S., Verwichte, E., Foullon, C.: 2012, First observation of a transverse vertical oscillation during the formation of a hot post-flare loop. *Astron. Astrophys.* **545**, A129. [DOI](#).
- Yokoyama, T., Akita, K., Morimoto, T., Inoue, K., Newmark, J.: 2001, Clear evidence of reconnection inflow of a solar flare. *Astrophys. J.* **546**(1), L69. [DOI](#).
- Zimovets, I.V., Nakariakov, V.M.: 2015, Excitation of kink oscillations of coronal loops: statistical study. *Astron. Astrophys.* **577**, A4. [DOI](#).

**Publisher's Note** Springer Nature remains neutral with regard to jurisdictional claims in published maps and institutional affiliations.

Springer Nature or its licensor holds exclusive rights to this article under a publishing agreement with the author(s) or other rightsholder(s); author self-archiving of the accepted manuscript version of this article is solely governed by the terms of such publishing agreement and applicable law.